REPORT DOCUMENTATION PAGE

Form Approved
OMB No. 0704-0188

1. AGENCY USE ONLY (Leave blank)	2. REPORT DATE	3. REPORT TYPE AND DATES COVERED
		* Final 1 Jun 94 - 31 May 97

4. TITLE AND SUBTITLE
Polymer-Based Integrated Photonic Devices for Highly Parallel Optical Interconnects

5. FUNDING NUMBERS
Grant #
F 49620-94-1-0321
1651/01
62173C

6. AUTHOR(S)
Charles Lee & Ray T. Chen

7. PERFORMING ORGANIZATION NAME(S) AND ADDRESS(ES)
The University of Texas at Austin
Microelectronics Research Center
MER 1.606 Bldg. 160
Austin, TX 78712-1100

8. PERFORMING ORGANIZATION REPORT NUMBER
AFOSR-TR
97-0725

9. SPONSORING/MONITORING AGENCY NAME(S) AND ADDRESS(ES)
AFOSR/NL
110 Duncan Avenue Rm. B-115
Bolling AFB DC 20332-8080

10. SPONSORING/MONITORING AGENCY REPORT NUMBER

11. SUPPLEMENTARY NOTES

12a. DISTRIBUTION/AVAILABILITY STATEMENT
Approved for public release;
distribution unlimited.

12b. DISTRIBUTION CODE

13. ABSTRACT *(Maximum 200 words)*

We have solved the crosslinker crystallization problem which has been a major bottleneck for several years. A new method of electro-optic measurenment is invented which has the advantageof being able to accurately measure r33 and r13 separately with a high accuracy. A theory of TE-TM mode conversion in tilted-poled NLO waveguides is developed. A new polarization-independent Mach-Zehnder modulator is designed and fabricated by using this theory. This device uses continuous modulation electrodes, thereby allowing the employment of traveling-wave modulation to achieve extremely high speed. Primary polarization-independent devices and directional-coupler devices have been fabricated. further design and fabrication of new high-performance electro-optic devices are under investigation.

19971217 005

14. SUBJECT TERMS

15. NUMBER OF PAGES

16. PRICE CODE

17. SECURITY CLASSIFICATION OF REPORT	18. SECURITY CLASSIFICATION OF THIS PAGE	19. SECURITY CLASSIFICATION OF ABSTRACT	20. LIMITATION OF ABSTRACT
unclassified	unclassified	unclassified	UL

POLYMER-BASED INTEGRATED PHOTONIC DEVICES FOR HIGHLY PARALLEL OPTICAL INTERCONNECTS

1996-1997 Annual Report
Contract No. F49620-94-1-0321

Presented to

Dr. Charles Y-C. Lee
AFOSR/NC

Presented by

Dr. Ray T. Chen
Microelectronics Research Center
University of Texas, Austin
Austin, TX 78758

CONTENTS

1. Introduction

Last year we solved the solvent compatibility problem for LD-3 polymer and made the first channel waveguides from this polymer. We also invented a new poling method--high temperature liquid contact poling (HTLCP)–which is an important contribution to the development of nonlinear optical polymers. The work of this year is an continuition of what we did last year. We have solved the crosslinker crystallization problem which has botherd other researchers for several years. A new method of electro-optic measurenment is invented which has the advantageof being able to measure r_{33} and r_{13} separately with relative high accuracy. A theory of TE–TM mode conversion in tilted-poled NLO waveguides is developed. A new polarization-independent Mach–Zehnder modulator is designed by using this theory. This device uses continuous modulation electrodes, thereby allowing to use traveling-wave modulation to achieve extremely high speed. Primary polarization-independent devices and directional-coupler devices have been fabricated. Design and fabrication of new high performance electro-optic devices are under way.

2. Improved Optical Quality of Crosslinkable Nonlinear Polymer Waveguides by Anchoring the Diffusive Small Molecules

2.1 INTRODUCTION

Using nonlinear optical (NLO) polymeric materials to fabricate electrooptic (EO) devices has several well recognized advantages such as compatibility with different substrates, ease of fabrication and possibly low costs compared with the inorganic counter parts such as lithium niobate. As a result, a lot of NLO polymers have been synthesized in recent years[2.1-2.5]. However, the progress of the fabrication of practical devices has been impeded by the lack of processability of the materials. A low loss waveguide with a high and stable NLO coefficient is needed for any practical device. Polyimide NLO materials offer the best stability; however, the NLO active materials have relatively high optical losses (>3dB/cm) and it is often the case that the losses and processability remain unreported[2.2]. Other materials, however, do not possess a thermal stability satisfying commercial or military requirements[2.6]. Much higher stability can be achieved by crosslinking both of the ends of a NLO chromophore into the polymer network. Although many efforts have been made, only a few NLO materials have achieved long term stabilities near or up to 100 ^{o}C[2.1-2.3,2.5] and one material (LD-3) turns out to have a long term thermal stability satisfying the military requirement of 125 ^{o}C[2.4]. LD-3 is a thermally

crosslinkable NLO polymer consisting of a poly (methyl methacrylate) (PMMA) backbone and an azobenzene-sulfone chromophore (figure 2.1(a)). It can be crosslinked by a diisocyanate crosslinker. Using Dianisidine diisocyanate (Pfaltz &Bauer, Inc.) as the crosslinker (figure 2.1(b)), a r33 value of 13pm/V at 633 nm was achieved and a long term stability at 125 ^{o}C is proved through annealing a sample at this temperature for over 1250 hours[2.7].

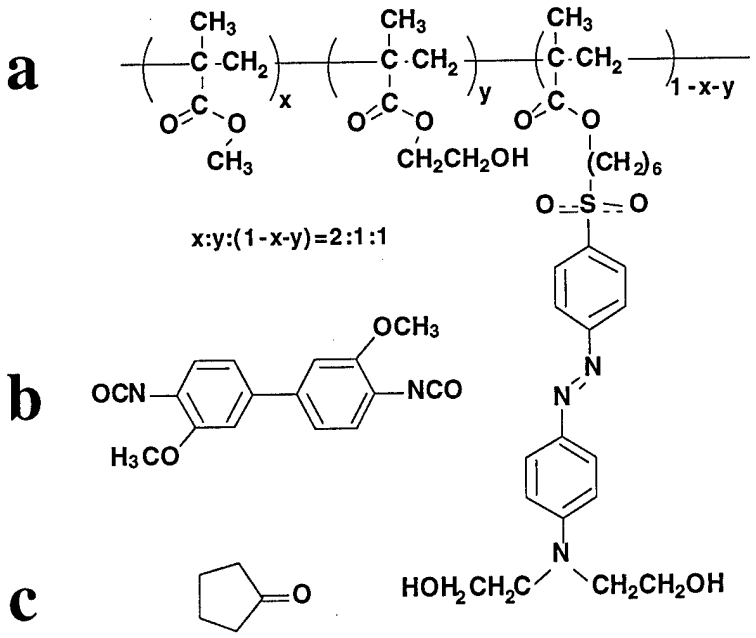

FIGURE 2.1. (a) the structure of the LD-3 polymer (b) the diisocyanate crosslinker (c) the cyclopentanone.

It is both technically and commercially interesting to use crosslinkable NLO polymer to fabricate EO devices. However, only very few materials have been reportedly used in making any kind of useful devices[2.3,2.5,2.8,2.9]. The excellent stability and the good EO coefficients make LD-3 polymer an ideal candidate for fabrication of EO polymer devices, but some unsolved processing problems with this material impede the progress of its practical application. Even some researchers who first published this material turn their attention to other materials which have much inferior stability[2.4,2.8,2.9]. The PURDR19 is most frequently used to fabricate waveguide device[2.8,2.9]. Test devices made of other two materials BIN2-HDT and Red-acid Magly are also reported by other researchers. However, BIN2-HDT, PURDR19 and Red-acid Magly have long term stabilities only up to 100^{o}C, 90 ^{o}C and 85 ^{o}C respectively.

It is significant if the processing problems of LD-3 can be solved because its superior stability allows a much wider range of applications. More importantly, some insight into these

problems might also apply to other crosslinkable NLO polymer systems. The key part of fabricating LD-3 based NLO polymer devices is the preparation of the NLO polymer films. For a crosslinkable polymer, we need to first dissolve the polymer and the crosslinker together to make a spin-coatable solution. Then the chromophores need to be aligned into a noncentrosymmetric order to obtain second order nonlinearity. The alignment of the chromophores is accomplished by applying a high electric field across the film while heating the film to above the glass transition temperature Tg of the polymer. The fix of the alignment is realized by crosslinking both of the ends of a chromophore into the polymer network at an elevated temperature.

2.2 ANCHORING THE CROSSLINKERS TO STOP THEIR CRYSTALLIZATION

After finding cyclopentanone to be a compatible solvent for LD-3, the crystallization of the crosslinker on the film surfaces was another obstacle. This phenomenon also bothers other researchers working on the same material. Figure 2.2 (a) shows a microscope picture of the crosslinker crystal grains formed on a LD-3 film surface. The crystals form tree branch patterns on the polymer surface. Usually there are more crystals formed along the edge of the silicon wafer than at the center.

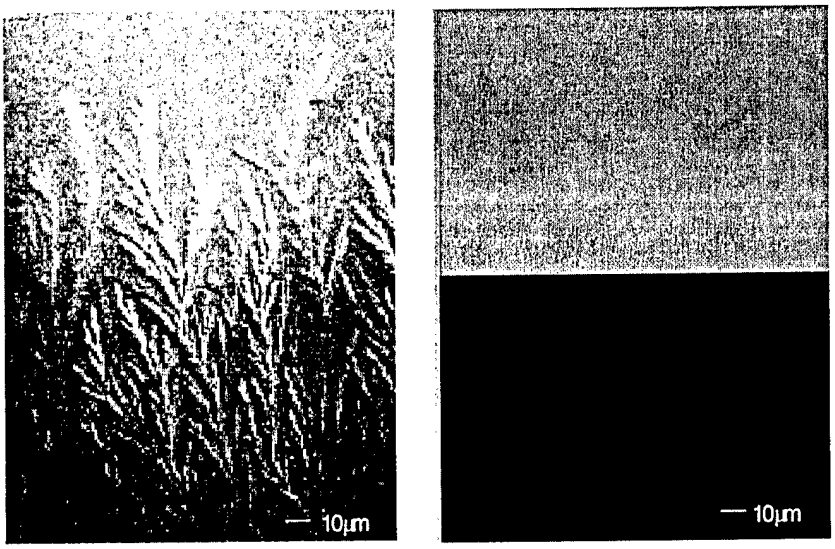

FIGURE 2.2. Microscope view of the LD-3 polymer films: (a) high solvent evaporation speed results in crystal grains; (b) low solvent evaporation results in smooth films (upper part: LD-3 on metal, lower part: LD-3 on glass)

In extreme cases, the tree shape pattern can cover areas of several square centimeters in total along the edge. We have tried other substrates, including glass slides, metals, polymers, but the crystallization always occurs. Therefore, it is not a problem of substrates. To solve this problem we carefully investigate when the crystallization occurred. We observed that no crystals appear just after the spin coating. The grains are formed during drying of the film in the vacuum. This indicates that the crystallization occurs when the solvent is being removed from the film and there is a phase segregation between the polymer and the crosslinker during this process. The role of the solvent in the crosslinker crystallization is not clear, but the phase segregation is dictated by the free energy of the system of the crosslinker and the polymer. If the crystallization of the crosslinker lowers the free energy of the system, it will occur no matter what solvent is used. This means the solid solubility of the crosslinker in the LD-3 polymer is low. One way to solve this problem is to reduce the crosslinker to polymer ratio. However, the ratio is determined by the stoichiometry of the crosslinking reaction and does not allow change. Another way is to use other crosslinkers which might have higher solid solubility in LD-3 polymer. Since this will change the composition of the resulted NLO films, the stability of the NLO properties might also change. Other crosslinkers tested do result in inferior stability[2,7].

The slow reaction between the polymer and crosslinker in the solution gives a clue fas how to solve this problem. Clearly there are three competing processes: the polymer -crosslinker reaction, the solvent evaporation and the crosslinker diffusion and crystallization. If the polymer-crosslinker reaction rate could consume enough crosslinkers so that the concentration of the free crosslinkers could be maintained lower than the solubility of the crosslinker in the polymer-crosslinker-solvent system during the solvent evaporation process, then the crosslinker would not crystallize. The simplest way to do this is by slowing down the solvent evaporation speed during vacuum drying. However, there might be another problem. Once the crosslinker has had enough time to react with the polymer, most of the chromophores might be crosslinked before poling, so the r33 value might be drastically reduced. There might be a possibility that only one of the two ends of a crosslinker has reacted to the LD-3 polymer within a certain length of time so that the segregation of the crosslinker is not possible, but the chromophore can still be aligned to the electric field because a crosslinking bridge forms only when both of the ends of a crosslinker are reacted. Statistically it is not possible to have all the crosslinker have only one end reacted. However, if the crosslinking density is very low (for example, <1%), there will be no appreciable decrease in the EO coefficient. Different levels of vacuum, from 10^{-2} torr to 1 torr, are used to control the evaporation rate. When a vacuum of 1 torr is used, good films free from crystal dots of the crosslinker are consistently obtained, when observed under microscope. For higher vacuum, some crystal dots always appear on the film surface. Of course longer drying time is

needed when the vacuum is lower. About 48 hours are needed to totally dry the films with 1 torr vacuum. The measurement of the EO coefficients show that this method causes no observable decrease in the r33 value. We obtain r33 values around 16pm/V in corona poled films at the wavelength of 633nm which is at least as good as the previously reported one at the same wavelength (13pm/V). Directly measuring the crosslinking density is difficult and is beyond our interest. The resulting r33 values indicate that the unwanted crosslinking density should be very low. An insight into the method can be obtained if we analyze microscopically the drying process. Figure 2.3 shows the microscopic mechanism of anchoring the crosslinkers. The crosslinker has a high mobility with the presence of the solvent so that it has a great chance to encounter the crosslinkable sites within the polymer matrix. Once one end is attached to the backbone, the mobility of the crosslinker is drastically reduced. As a result, the probability for the second end of a crosslinker to encounter a crosslinkable site is much smaller. Therefore, it is possible to have most of the crosslinkers anchored to the polymer but without forming many crosslinked bridges. This is difficult to be realized in a solution. First, the polymer chains can move in the solution, so there might still be a considerable chance for the second end of a crosslinker to encounter a crosslinkable site associated with another backbone. More importantly, the solution will turn into a non-spincoatable gel as mentioned before even if there is only a small amount of crosslinking. However, the motion of the polymer is greatly reduced due to the loss of most of the solvent and the large molecular size of the polymer after the solution is spin-coated onto the substrate and a film is formed. Therefore a well controlled evaporation rate will ensure that most of the diffusive crosslinkers are attached to the polymer while most of the chromophores can still have the rotational freedom. There is no report of any kind of crystallization in the previous mentioned NLO polymers. This is not unexpected. No crosslinker is used with the Red-acid Magly. For the other two materials, a precuring is conducted after the crosslinker is added. Although no one reported why a precuring step is necessary, we can understand that precuring has combined small molecules into larger molecules, hence the precipitation of any small molecules is prevented. Because the starting materials of PURDR19 or BIN2-HDT are all small molecules with molecular weights of a few hundred atomic units, a well controlled precuring will not turn the polymer solution into a non spin coatable gel. On the other hand, the average molecular weight of LD-3 polymer is expected to be at least tens of thousands atomic units. Precuring before spin-coating is not viable in LD-3 polymer for the reason mentioned before. Through this comparison we can see that the slow evaporation of the solvent plays the same role as the precuring step in the other polymers, but it happens after spin coating.

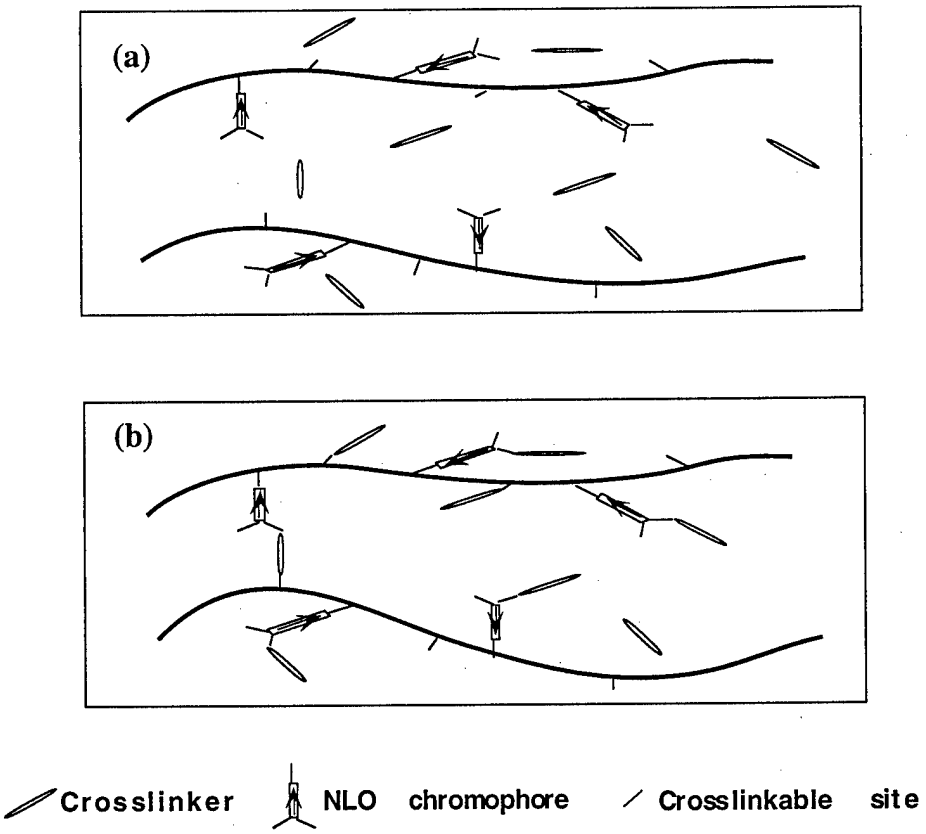

FIGURE 2.3. Mechanism of anchoring the crosslinker. (a) free crosslinker can diffuse and crystallize out; (b) slow evaporation rate allows a crosslinker to have time to attach one end to the polymer backbone, but the second end of a chromophore has much less chance to encounter a crosslinkable site.

Polymer films prepared in this way show no observable crystallization, regardless of what substrates were used. The films prepared on silicon wafer were very smooth and featureless under microscope observation. To show some contrast, we prepared a film on a microscope slide with chromium patterns. Figure 2.2 (b) is a microscopic picture of the film. The upper part of the film is on chromium, so it is bright due to the reflection. The lower part is on glass, so it is darker due to the transparency of the glass and the film.

2.3 LOSS MEASUREMENT AND CONCLUSION

The ultimate check of the effectiveness of the film preparation method is the waveguide losses. A multilayer planar waveguide on a 4-inch silicon wafer is fabricated. First an aluminum

layer is deposited as the ground electrode. Then 3 μm optical adhesive NOA61 is coated as the lower cladding, then 1.2 μm LD-3 polymer, and finally 1μm of NOA61 as the upper cladding. An infrared light with a wavelength of 1.32μm is coupled into the waveguide from a prism located at the center at the wafer. The propagation of the light from the center of the wafer to the edge is clearly observed using a CCD camera. It propagates nearly 5 cm and then emerge from the wafer edge. The loss is determined by measuring the scattered light intensity along the light streak[10]. Figure 2.4 shows the loss measurement result. Relatively low loss of 1.3dB/cm is achieved. Lower loss (less than 1dB) can be expected if the core and the lower cladding thicknesses are increased. There is no reported loss data of LD-3 polymer. Compared with other reported results in NLO polymers[3,9], this loss is acceptable.

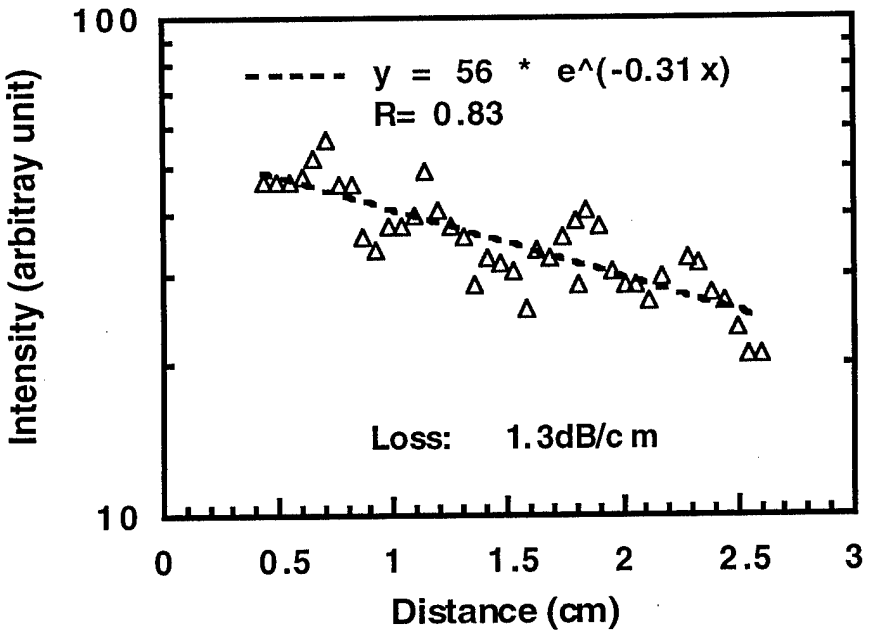

FIGURE 2.4. Optical loss measurement of a planar LD-3 polymer waveguide with NOA 61 as the cladding material.

In conclusion, the crosslinker crystallization problem has been solved by balancing the polymer-crosslinker reaction rate and the solvent evaporation rate. The different reaction probabilities of the two ends of a crosslinker resulting from the reaction sequence is understood as the underlining mechanism. Good optical quality multilayer planar waveguides with relative low loss have been fabricated. Although this discussion is limited to LD-3 polymer, the same principle can be applied to fabricate other polymer films involving the use of a crosslinker. Based on the mechanism discussed, the processing time might be shortened by using different drying schemes. This investigation is in progress.

3. Novel Poling and Electro-Optic Measurement Methods of Cladded Nonlinear-Optical Polymer Films

3.1. INTRODUCTION

Almost all the applications of nonlinear-optical (NLO) polymers requires one to form the polymers into some kind of a waveguide. Such waveguides usually use an NLO polymer as the core material and use other materials with lower refractive index as the top and bottom cladding layers. Therefore, poling efficiently cladded NLO polymer films and being able to measure quickly the electro-optic (EO) coefficients are very important for development of NLO polymer devices. Using electrode-contact poling to induce nonlinearity in cladded NLO films[3.1,3.2] has been studied by some researchers. However, the newly developed poling method known as high temperature liquid contact poling (HTLCP) has not yet been applied to pole cladded NLO films.

To study the poling effect of this new poling scheme, a method that can quickly and reliably measure the EO coefficient is needed. A widely used method of EO measurement of NLO polymers is an ellipsometric method[3.3,3.4]. This ellipsometric method may be not applicable to a cladded NLO polymer film because the assumption made in deducing the formula for relating the EO coefficient to the measured quantity of measurement is not necessarily applicable to a cladded NLO film owing to the multiple reflections from all the interfaces. New methods have been reported in recent years[3.5-3.8]. These methods either require special design of modulation or poling electrodes or are just an extension of the ellipsometric method and are not suitable to measure the EO coefficients of a cladded NLO polymer film. As a result, the amount of work needed to measure the EO coefficient of a cladded NLO film is almost the same as that of preparing and characterizing an EO device by interferometric means which requires the time consuming processes of polishing and coupling.

In the first part of this chapter, we report the primary result of using the HTLCP method to pole efficiently cladded NLO polymer films. In the second part, we at first demonstrate the inapplicability of the ellipsometric methods to cladded NLO polymer films experimentally, and then present both a theoretical analysis and some experimental results on this new EO-measurement method.

3.2. HIGH TEMPERATURE LIQUID-CONTACT POLING AND ITS APPLICATION TO POLING CLADDED WAVEGUIDES

Poling is a critically important processing step in preparing nonlinear optical polymer devices. The value of the electro-optic coefficient r_{33} of an NLO-polymer film depends on the polarization density achieved after the electric-poling process. To date, two common methods of electric-field poling are contact poling and corona poling. In contact poling, a strong electric field is applied to the cladded NLO polymer film by two parallelplate electrodes. These poling electrodes cover large areas and provide a path of high lateral conductivity. Such an arrangement frequently generates a localized destructive current at certain location with pinhole defects. A single defect created during film processing may introduce a catastrophic short circuit, and thereby destroy the device. As a result, contact poling in most cases can only be performed at a field strength much lower than the dielectric strength of the NLO polymer. In corona poling, a high electric field is produced by the charge deposited on the film surface through the corona discharge process. A poling electric field close to dielectric breakdown can easily be obtained[3.9]. Larger poling fields activate larger nonlinearities compared with contact poling; however, surface damage is a major concern in corona poling.[3.10] To overcome the problems with these two methods, we have developed a high temperature liquid-contact poling method[11] that avoids the disadvantages of the other two methods and, hence, makes it possible to apply very high poling electric fields, while keeping the surface damage density low.

The NLO material used in the experiment is LD-3 and is available commercially. It is a thermally crosslinkable polymer consisting of a poly (methyl methacrylate) (PMMA) backbone and an azobenzene-sulfone chromophore. The cladding material NOA61 is a UV curable optical adhesive which is bought from Norland Products, Inc. The choice of UV curable cladding material was made because the curing process does not need heating. Any heating before poling might partially crosslink the polymer, which would result in limiting the alignment of the chromophores with the poling electric field, the induced optical nonlinearity would thus be reduced. The details of preparing LD-3 polymer waveguides is reported elsewhere[3.12]. Silicon is used as the substrate with gold deposited on the silicon surface to form a bottom electrode. The bottom cladding, LD-3 film, and top cladding are sequentially deposited by solution spincoating. The thickness of the bottom cladding and LD-3 polymer is measured by an Alpha-Step 200 surface profiler to be 3 μm, 1.2μm respectively, The thickness of the top cladding can be varied for different applications. The process of preparing the liquid-contact-poling cell which contains the cladded LD-3 film is the same as that for a LD-3 single layer[3.11]. Epoxy spacers are used to maintain a gap between the top cladding and the top electrode. The contact liquid, hexatriacontane, is a solid at room temperature and melts at 75°C. When it melts, its resistivity becomes much lower. Before raising the temperature of the sample, we place this material at the edge of the sample. When the melting point is

reached, it becomes a liquid and is sucked into the gap by capillary action with no bubble formation. As a result, an electrically conductive path between the upper electrode and the polymer film is formed through the liquid layer. Most of the voltage applied to the electrodes will drop across the polymer films as long as the resistivity of the contact-liquid layer is much lower than that of the LD-3 polymer film. A high breakdown voltage of the contact liquid is necessary to insure that a high poling field can be applied. If there is any local breakdown in the polymer film, the contact liquid can still prevent a short circuit. Although the poling current might increase, it would not be significant as long as any local breakdown is limited to very small areas.

In the previous report, the samples used in the experiments only had a layer of the nonlinear optical polymer. There were no cladding layers. The poling liquid contacted directly with the top surface of the NLO polymer. Figure. 1(a) shows the configuration of a poling cell for liquid -contact poling where there is only an NLO polymer layer. A poling voltage of 300 volts can be safely applied to this cell. This high voltage drops directly across the 1.2 μm NLO film, so that the applied electric field should be 250 V/μm, which is comparable to the reported value of the corona-poling electric-field strength. For fabrication of any real device, however, a bottom cladding has to be deposited before coating with the NLO polymer. The top cladding can be coated on before or after poling. There are certain advantages placing the top cladding before poling. First, the top cladding separates NLO film from the temporary contact liquid used during the poling step, so less surface damage is expected. Secondly, the buffering effect of the cladding may allow application of even higher poling electric-field strength, which would improve the poling efficiency. Fig.3.1(b) shows a poling cell of a cladded NLO film with both the bottom and top claddings.

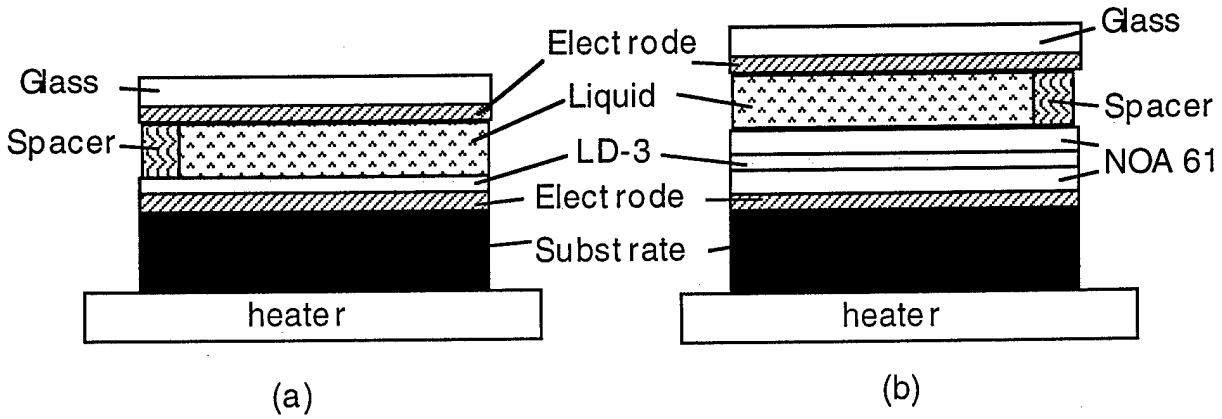

FIGURE 3.1 The structures of high-temperature liquid-contact poling cells. (a) A cell with only an LD-3 layer
and (b)a cell with a cladded LD-3 waveguide.

Our experimental results indeed confirm that a poling voltage higher than 300 volts can be applied to a poling cell of a cladded NLO polymer film. Poling voltages of 400 volts have been successfully used to pole several samples. Even higher poling voltages can be applied without causing a short circuit. The highest voltage tested is 500 volts. Although no short circuit occurs at this high voltage, some burn spots do appear on the film.

A high poling voltage applied to a cladded-NLO-film cell is expected to generate a high EO coefficient if the cladding layers have much lower resistivity than the core material at the poling temperature. How effective the poling process is can only be determined by measuring the EO coefficient of the poled film. The ellipsometric method is routinely used to measure the EO coefficient of a single-layer NLO film. However, this method does not give consistent results for cladded NLO waveguide films we have measured. We realize that the error caused by multilayer reflections might be too large and that it could neither be ignored nor removed.

The lack of a reliable method to measure quickly EO coefficients inspired us to search for a new way to do the measurement. It happens that a sample prepared for another purpose has a slightly tilted top electrode. Although this sample is not poled optimally (poled at 190V), it allows us to investigate the effect of the thickness variation of the top cladding on the EO measurement. Further theoretical analysis leads us to propose the following new method of EO measurement.

3.3. NOVEL METHOD OF MEASUREING THE ELECTRO-OPTIC COEFFICIENTS OF CLADDED WAVEGUIDES

Our calculation of the amplitudes of the reflected light from each of the different interfaces of our sample shows that error in the EO measurement of a cladded NLO film by the ellipsometric method can come from the interference of the light reflected by all the interfaces. The amplitude and phase of the reflected light are each sensitive to the thickness of each layer of the sample. We confirm this conclusion experimentally by using the sample mentioned at the end of last section. Figure 3.2(a) shows a schematic of the sample. The tilted top electrode is attached to the top surface of the cladded waveguide by the

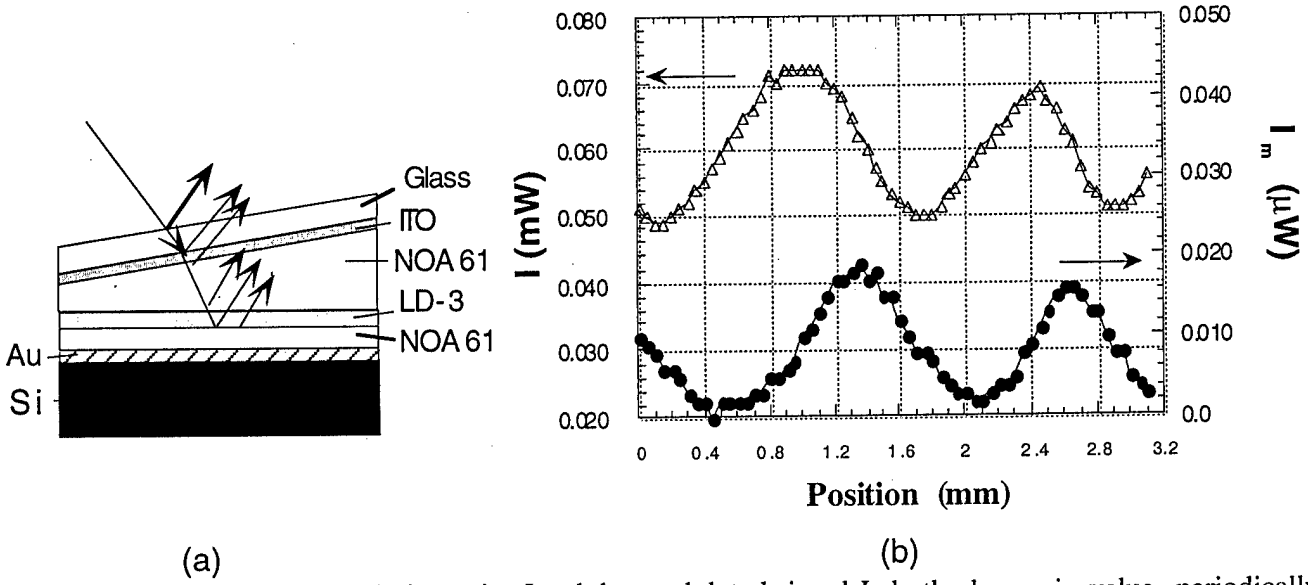

FIGURE 3.2. The reflected light intensity I and the modulated signal I_m both change in value periodically with increases in the top-cladding thickness. (a) A schematic of the sample with varying top-cladding thickness and (b) measured I and I_m curves

same material used as the cladding , which is NOA 61. The resulting sample is a waveguide, where the thickness of the top cladding layer varies with position. The incident angle of the light is set at 45 degrees in the measurement. A modulation signal of 50 V (rms) at 1kHz is applied to drive the EO response of the sample. The measured reflected light intensity I and modulated portion I_m vary periodically with position. Every period corresponds to a phase change of the optical path by 2π or 0.18 μm in thickness of the cladding ,which is calculated using n=1.56 for the cladding refractive index at 633 nm.

In the ellipsometric method, the change in the phase-difference between the *p*-wave and the *s*-wave owing to electro-optic modulation is determined by measuring the ratio of I/I_m. The EO coefficient r is then derived from the change in this phase difference. One important feature of the deduced formula in the references[3.3,3.4] is that the phase change is independent of the thickness of the film. We can see from Fig. 3.2(b) that the ratio of I/I_m is also a periodic function of the top cladding thickness as I and I_m are, so the simple formula used in the ellipsometric method is not applicable to our samples which have a cladded film. To extract EO coefficients from the two curves in Fig. 3.2 (b) is not an easy job because I and I_m involve the interference effect of many beams.

However, using pure *p*-polarized or *s*-polarized light can simplify the situation. The reflected light from all the interfaces can be sorted into three groups according to their phase properties. The first group is the light reflected from all the interfaces above the top cladding. The phase of this group is not dependent on the cladding or NLO film thickness. The second group only includes the light reflected from

the interface between the top cladding and the NLO polymer. The phase retardation of this group is dependent on the top cladding thickness only. The third group includes all the light that passes through the NLO film. The phase retardation of this third group is a function of both the top cladding thickness and the modulation voltage, which induces a change in the refractive index of the EO polymer. The complex amplitude of reflected light can be written as the sum of the three groups

$$E = E_1 e^{i\varphi_1} + E_2 e^{i\varphi_2} + E_3 e^{i\varphi_3}, \tag{3.1}$$

where E_1, E_2 and E_3 denote the absolute values of the amplitudes of the electric field of the light of the three groups as shown in Fig. 3.3 (a), and φ_1, φ_2, and φ_3 are the corresponding phases.

The phase properties of the three groups of light can be expressed mathematically as

$$\varphi_1 = constant, \tag{3.2a}$$
$$\varphi_2 = \varphi_2(d_{cl}), \tag{3.2b}$$
$$\varphi_3 = \varphi_3(d_{cl}, V), \tag{3.2c}$$

where d_{cl} is the top cladding thickness and V is the modulation voltage. Equation (3.2) indicates that the reflected light intensity

$$\begin{aligned} I &= EE^* \\ &= E_1^2 + E_2^2 + E_3^2 + 2E_1E_2\cos(\varphi_2 - \varphi_1) + 2E_2E_3\cos(\varphi_3 - \varphi_2) + 2E_3E_1\cos(\varphi_3 - \varphi_1) \end{aligned} \tag{3.3}$$

is also a function of d_{cl} and V. The top transparent electrode, which is made of indium tin oxide (ITO), has the high refractive index of n=2.0, so the reflectivities of the interfaces between the ITO and the glass or NOA61 are large. The refractive indices of the cladding and the core are quite close, so the E_2 is relatively weak. The ratio of E_3:E_1:E_2 is on the order of 100:10:1, so that the reflected light intensity is approximately

$$I \approx E_1^2 + E_3^2 + 2E_3E_1\cos(\varphi_3 - \varphi_1). \tag{3.4}$$

Equation (3.4) gives

$$2E_3E_1 = \frac{1}{2}(I_{\max} - I_{\min}), \tag{3.5}$$

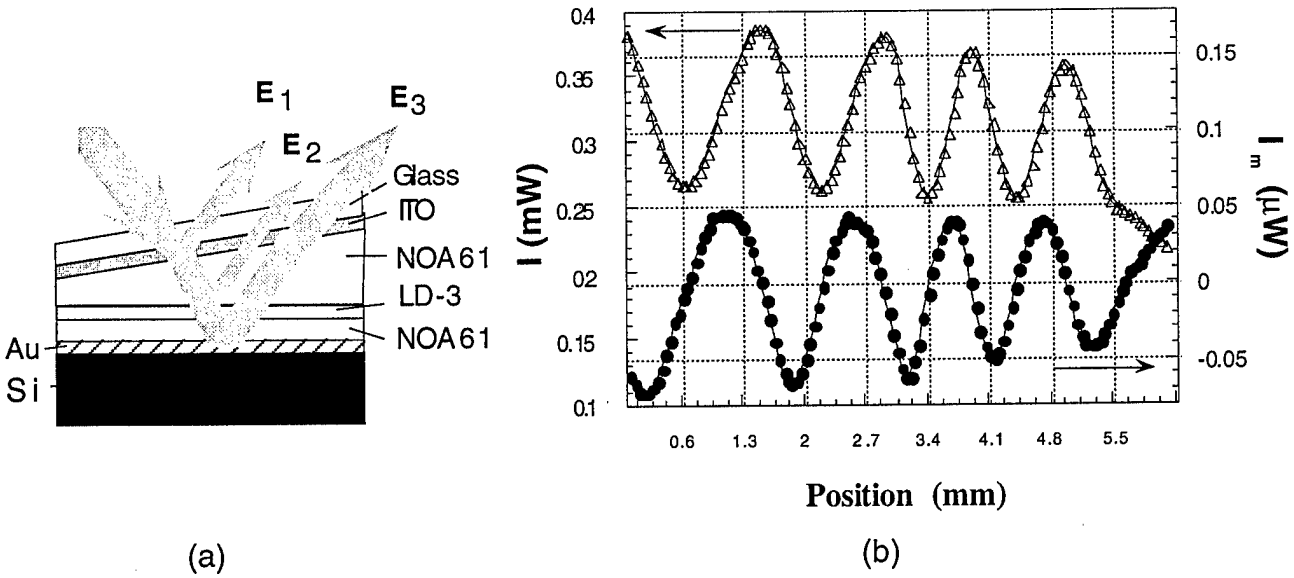

FIGURE 3.3. The reflected light intensity I and the modulated intensity I_m are functions of the top-cladding thickness owing to interference . (a) Three groups of the reflected light and (b) measured I and I_m curves.

where I_{max} and I_{min} are the maximum and minimum of the reflected light intensity, respectively. The modulated signal is

$$I_m = \frac{dI}{d\varphi_3}\Delta\varphi_3 = -2E_3E_1\sin(\varphi_3-\varphi_1)\Delta\varphi_3 - 2E_3E_2\sin(\varphi_3-\varphi_2)\Delta\varphi_3. \tag{3.6}$$

Changes in top-cladding thickness will not affect the phase difference $(\varphi_3-\varphi_2)$, so the second term in Eq. (3.6) can be subtracted out. The maximum and minimum of the modulated signal are

$$I_{m,\max} = 2E_3E_1\Delta\varphi_3 - 2E_3E_2\sin(\varphi_{3\max}-\varphi_2)\Delta\varphi_3, \tag{3.7}$$

$$I_{m,\min} = -2E_3E_1\Delta\varphi_3 - 2E_3E_2\sin(\varphi_{3\max}-\varphi_2)\Delta\varphi_3. \tag{3.8}$$

Subtracting Eq. (3.8) from Eq. (3.7) gives

$$2E_3E_1\Delta\varphi = \frac{1}{2}(I_{m,\max}-I_{m,\min}). \tag{3.9}$$

Equation (3.5) and (3.9) give

$$\Delta\varphi = |\Delta\varphi_3| = \frac{I_{m,\max}-I_{m,\min}}{I_{\max}-I_{\min}} \tag{3.10}$$

Using Eq. (3.10), we can calculate the phase change induced by the drive voltage.

A schematic of the experiment setup is shown in Fig. 4. We use p-polarized light with an incident angle of 45° and a modulation voltage of 50 V (rms). A translation stage is used to move the sample. The

measured variation of the light intensity I and EO-modulated signal I_m with position is shown in Fig. 3(b). The maxima and minima of these curves are used to calculate the phase modulation $\Delta\varphi$ according to Eq. (3.10) and the results are plotted in Fig. 5. The scatter of the data points is less than ±10%, so this method gives much more reliable results than the ellipsometric method.

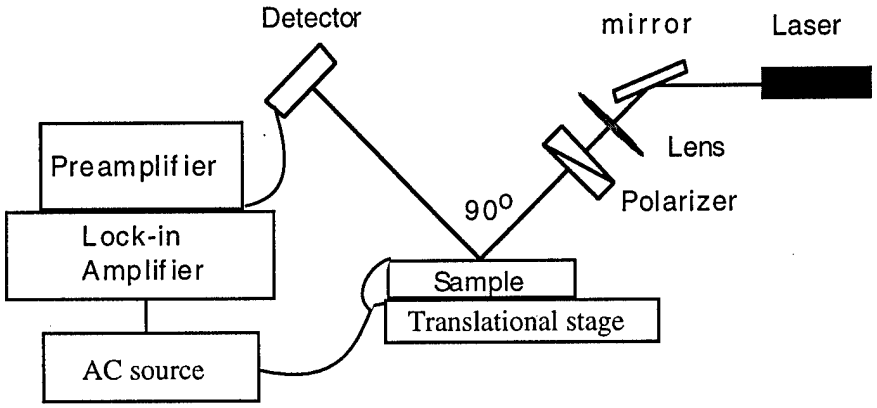

FIGURE 3.4. Schematic of the experiment setup.

The effective EO coefficient r_{eff} can be calculated from the phase modulation by

$$r_{eff} = \frac{\lambda d \cos\alpha}{\pi n^3 d_{NLO} V} \Delta\varphi, \tag{3.11}$$

where α is the angle of incidence measured in the NLO polymer, d_{NLO} is the effective thickness of the NLO polymer, and d is the distance between the electrodes, which varies with position. One can see that $\Delta\varphi$ is inversely proportional to the distance between the two electrodes for a uniformly poled film, i.e. $\Delta\varphi$ decreases when d increases. This trend is clear in Fig. 5 . When d is much larger than the wavelength of light in the cladding, r_{eff} can be estimated by the average value of d. The value of r_{eff} is related to r_{33} and r_{13} by

$$r_{eff} = r_{33} \sin^2\alpha + r_{13} \cos^2\alpha \tag{3.12}$$

for p-wave, and

$$r_{eff} = r_{13} \tag{3.13}$$

for s-wave.

Using Eqs. (3.10) and (3.11) we should be able to calculate r_{eff} if the average electrode-to-electrode distance is known. From the data in Fig. 5 we estimate that r_{33}=10.7 pm/V at 633nm assuming $r_{33}=3r_{13}$

and using an average value of d being 8 μm. The 8 μm electrode-to-electrode distance is estimated from the sample fabrication process. More accurate result can be obtained by directly measuring d. Considering the poling voltage of 190V, the r_{33} value is in a reasonable range compared with previously reported data.

However, the assumption that $r_{33}=3r_{13}$ is not necessary for this method according to Eqs. (3.12) and (3.13). The values of r_{33} and r_{13} can be determined by applying sequentially a p-wave and a s-wave to probe the EO response. We find the ratio of r_{33} to r_{13} is 3.25, which is larger than but close to 3.0.

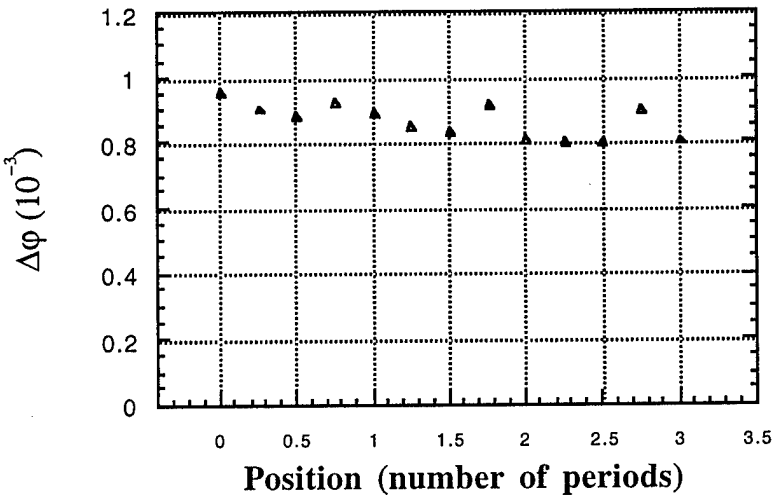

FIGURE 3.5. Induced phase change s deduced from Figure 3.

3.4. DISCUSSION

Equations (3.3) and (3.6) predict that the I and I_m curves be 90° out of phase with each other, which is consistent with the experimental observation and is clearly shown in Fig. 3. These equations also indicate that the electric field E_2 is an error source in our measuremnt. Its influence on I comes from the 4th term in Eq. (3.3), which is on the order of E_2/E_3 times $I_{max}-I_{min}$. It affects strongly the curve shape of I_m and is responsible for the asymmetry of the curve with respect to $I_m = 0$. The magnitude of asymmetry caused by E_2 is relatively large and is on the order of E_2/E_1 times $I_{m,max}-I_{m,min}$ (see Eqs. (3.6)), but the effect of E_2 on the measurement of $I_{m,max}-I_{m,min}$ can be eliminated as shown by Eqs. (3.7)-(3.9). So the total

error caused by $E2$ in our experiment is proportional to E_2/E_3, which is typically on the order of 1%. The magnitude of E_2 is determined by the index difference between the cladding and the core materials, hence this error can be further reduced by reducing this difference.

One important advantage of our method is that the values of r_{33} and r_{13} can be determined separately without knowing the ratio of r_{33}/r_{13}. In the ellipsometric method, a ratio of $r_{33}/r_{13}=3$ is assumed. This assumption is only valid at a low poling electric-field strength. At a high poling electric-field strength, this ratio is larger than 3. This is true for our sample. The ellipsometric EO measurement method can not determine the values of r_{33} and r_{13} if the ratio of r_{33} to r_{13} is not available because it can only measure the difference between r_{33} and r_{13}.

The process to attach the top electrode to the waveguide by UV curable adhesive is simple. It is even simpler than any electrode-deposition method for a trained person. Therefore, our method may allow fast and reliable characterization of NLO polymer films. The measurement setup does not need a phase compensator, so it is also simpler to use than that of the ellipsometric method.

So far we have presented the primary theoretical analysis and experimental results of a new EO measurement method, which is applicable to cladded NLO films. More systematic studies of this method are in progress. Experimental comparison of the result of this method with that of other reliable methods is planned.

3.5. CONCLUSION

Using high-temperature liquid-contact poling, a poling voltage as high as 400 volts can be applied to a cladded NLO film. The lack of a quick method to characterize the cladded NLO films has inspired us to devise a new EO measurement method. This method makes use of the interference between the modulated light and the unmodulated light in the reflected beam used to probe the electro-optic response of the material. The variation of top cladding thickness required by this method can be achieved simply by using UV-curable optical adhesive to attach a tilted top electrode over the waveguide top cladding layer. Theoretical analysis and experimental results show this method to be promising . Further development of this method is in progress.

4. Analysis Of Poling Induced Birefringence On The Design Of Polarization-Independent Nonlinear Optical Polymeric Devices

4.1. INTRODUCTION

Nonlinear optical (NLO) polymeric materials have several well recognized advantages such as compatibility with different substrates, ease of fabrication, simple design for high-speed modulation and possibly low fabrication cost. Polymer electro-optic modulators with bandwidths of over 110 GHz have been demonstrated. The large bandwidth is possible owing to the low value of the dielectric constant of polymers which makes it easy to match the phase velocity between the microwave and the optical wave in an electro-optic device. For applications of polymer modulators or switches in fiber optic systems, polarization-independent operation is desired. This is because widely used low-loss single-mode fibers do not preserve the state of linear polarization. Even in some applications where polarization-preserving fibers can be used, it would be more expensive because the alignment of the polarization-preserving fiber with the waveguide is more difficult. As a result, different polarization-independent devices have been proposed[4.1,4.2]. However, all these devices require non-continuous electrodes. The noncontinuity of electrodes makes it difficult to use a traveling-wave microwave voltage to drive the device, hence, design limits are imposed upon the device modulation speed. Therefore, new polarization-independent devices with continuous-electrode structure are needed to exploit the full potential of NLO polymeric materials.

Poling-induced birefringence is an important property of NLO polymers[3]where the refractive index increases along the direction of the poling field, while the refractive index decreases along the directions perpendicular to the poling direction. This induced liner-optical birefringence can strongly affect the device operation, especially for the devices which are not uniformly poled throughout the NLO polymer film. Tilted electric field lines at the edges of the poling electrodes can result in a rotated optic axis which is no longer perpendicular to the substrate plane. This birefingence can cause conversion between a transverse electric (TE) mode and a tansverse magnetic (TM) mode. This conversion can be an inadvertent effect, but it can also be used to develop new device concepts which are not possible in inorganic NLO materials. In this paper, at first we deduce a set of analytic formulae of tilted-poling-induced TE–TM mode conversion and then we apply these formulae to design a new kind of polarization-independent device.

4.2. THEORY OF TE–TM MODE CONVERSION OWING TO TILTED-POLING-INDUCED BIREFRINGENCE

Mode conversion between transverse-electric modes and transverse-magnetic modes is caused by nonzero off-diagonal elements in the dielectric constant matrix ε. Many polymeric materials are isotropic, so there are no such terms. Some are anisotropic, but the principle axes of the refractive index are perpendicular or parallel to the film surface. The off-diagonal elements are thus all zero. Poling an NLO polymer causes microscopical rotation of the NLO chromophores into an alignment with the direction of the poling electric field, and hence induces a refractive index change. By tilting the poling electric field, we can generate nonzero off-diagonal elements. Fig. 4.1 shows a waveguide which consists of an input and an output region and a tilted poled region in the middle.

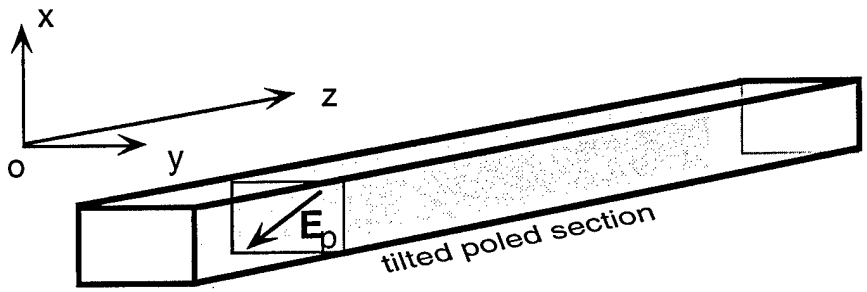

FIGURE 4.1. A waveguide with a tilted poled section

The matrix of the relative dielectric constant of the tilted-poled section can be expressed as

$$\varepsilon_r = \begin{bmatrix} \varepsilon_{11} & \varepsilon_{12} & \varepsilon_{13} \\ \varepsilon_{21} & \varepsilon_{22} & \varepsilon_{23} \\ \varepsilon_{31} & \varepsilon_{32} & \varepsilon_{33} \end{bmatrix} = \begin{bmatrix} n_1^2\cos^2\alpha + n_2^2\sin^2\alpha & (n_1^2 - n_2^2)\sin\alpha\cos\alpha & 0 \\ (n_1^2 - n_2^2)\sin\alpha\cos\alpha & n_1^2\sin^2\alpha + n_2^2\cos^2\alpha & 0 \\ 0 & 0 & n_3^2 \end{bmatrix}, \tag{4.1}$$

where $\alpha = \alpha(x,y)$ is the angle between the x-axis and the principle axis 1 of the refractive indicatrix of the poled region, $n_1 = n_1(x,y)$ and $n_2 = n_2(x,y)$ are the indices along the corresponding principle axes. The principle axis 1 is chosen to be parallel to the direction of the poling field. Thus axis 3 is parallel to z axis and axis 2 is perpendicular to the other two axes. The z-axis is the light-propagation direction. Generally, the magnitude and direction of the poling electric field are not uniform, so the resulting poling-induced birefringence is also nonuniform in both magnitude and direction.

One may solve the wave equations in the poled region by numerical methods[4.4,4.5]. But for a moderate poling-induced birefringence, we can use coupled-mode theory to obtain an analytic solution. Although the applicability of the analytic solution has its limitations, but it provides more insight into the effect of poling-induced birefringence than a numerical solution. Here we restrict ourselves to the most practical case where a waveguide supports only a single TE and a single TM mode. The waveguide could

be either a channel waveguide or a planar waveguide as long as it supports only a single mode for each of these polarization states. We use the eigenmodes of the unpoled waveguide section as basis, so we can expand a general input electrical field $\mathbf{E}=\mathbf{E}(x,y,z)$ as

$$\mathbf{E} = \mathrm{A}(z)\mathbf{E}_x(x,y,z) + B(z)\mathbf{E}_y(x,y,z) \tag{4.2}$$

in terms of the TM eigenmode $\mathbf{E}_x(x,y,z)$ and TE eigenmodes $\mathbf{E}_y(x,y,z)$, where $A(z)$ and $B(z)$ are expansion coefficients. In the input or output region, $A(z)$ and $B(z)$ are independent of z. As the light goes from the unpoled region to the poled region, the index change will cause coupling between these two modes. There is also the possibility of coupling among these two modes and the radiation modes that form the complete set of modes in the unpoled region, since the eigenmodes of the unpoled section are no longer eigenmodes in this section. As long as the coupling to the radiation modes is negligible, the expansion of Eq. (4.2) is strict. So the following discussion is thus restricted to the case where coupling to the radiation modes can be neglected, which greatly simplifies the formulation.

The vectorial wave equation

$$\nabla\times\nabla\times\mathbf{E} - \frac{\omega^2}{c^2}\varepsilon_{\mathbf{r}}\cdot\mathbf{E} = 0 \tag{4.3}$$

should be used for the poled region. Using the following substitution (see Appendix A)

$$A(z) = A'(z)e^{-i\kappa_{aa}z - i\delta z}, \quad \text{(4.4a)}$$

$$B(z) = B'(z)e^{-i\kappa_{bb}z + i\delta z}, \quad \text{(4.4b)}$$

we have

$$\mathbf{E} = [A'(z)E_x(x,y)\hat{\mathbf{x}} + B'(z)E_y(x,y)\hat{\mathbf{y}}]e^{i(\omega t - \bar{\beta}z)} \tag{4.5}$$

following Eq. (A12). Using coupled-mode theory[4.6] and the assumption that the waveguide is symmetric both in the horizontal and vertical dimensions, we can deduce that

$$A'(z) = \left(\cos(z\sqrt{\kappa^2+\delta^2}) - \frac{i\delta}{\sqrt{\kappa^2+\delta^2}}\sin(z\sqrt{\kappa^2+\delta^2})\right)A(0) - \frac{i\kappa}{\sqrt{\kappa^2+\delta^2}}\sin(z\sqrt{\kappa^2+\delta^2})B(0), \tag{4.6a}$$

$$B'(z) = -\frac{i\kappa}{\sqrt{\kappa^2+\delta^2}}\sin(z\sqrt{\kappa^2+\delta^2})A(0) + \left(\cos(z\sqrt{\kappa^2+\delta^2}) + \frac{i\delta}{\sqrt{\kappa^2+\delta^2}}\sin(z\sqrt{\kappa^2+\delta^2})\right)B(0), \tag{4.6b}$$

from Eqs. (A11) to (A17), where δ is half of the difference between the effective propagation constant of TE and TM modes as defined in the Appendix A, κ is the coupling coefficient between the TE and the TM modes that is defined by Eqs. (A15)and (A9), and $\bar{\beta}$ is the average propagation constant. Other symbols are defined by Eqs. (A9). The modulation in the refractive index n_1 and n_2 by applying electric field will cause the modulation of κ, κ_{aa}, κ_{bb}, $\bar{\beta}$ and δ, as a result the modulation of both the magnitudes and phases of the TE and the TM modes. The TE–TM conversion is controlled by κ and δ. Thus the modulation of κ and δ allows electro-optic control of the polarization conversion.

A change of the poling electrode offset can be used to tune the tilt angle of the electric field lines. For a certain offset giving δ=0,

$$A'(z) = A(0)\cos\kappa z - iB(0)\sin\kappa z, \tag{4.7a}$$
$$B'(z) = -iA(0)\sin\kappa z + B(0)\cos\kappa z. \tag{4.7b}$$

For waveguides with a square cross section, α should have a distribution centered at 45°. For other waveguides, the condition of δ=0 can be determined experimentally. Under the condition that δ=0, the modulation of δ is also negligible, because the terms in Eq. (A16) cancel each other.

4.3. POLARIZATION-INDEPEDENT MACH-ZEHNDER MODULATORS

4.3.1 Device structure

A single channel waveguide with tilted poling can be used either as a modulator or polarization converter. This kind of device is not polarization independent as one can see from Eqs. (4.7), but a proper combination of two of these poled waveguides into a Mach-Zehnder structure can achieve polarization-independent operation. The device structure is shown in Fig. 2.

From Eq. (4.1) one can see that, if α is replaced by 180°-α or 90°+α, ε_{12} will change sign and so will the coupling constant κ. By building a Mach-Zehnder structure, where the poling field used in one arm is a mirror image or rotation by 90° of the field in the other (Fig.4. 2(b)), polarization-independent

operation is achieved when δ=0. The amplitude of TE and TM modes at the output are the superposition of the amplitudes of TE and TM modes from the arm 1 and arm 2 respectively. If we assume that the amplitude of the TM and TE modes at the input are A_0 and B_0 respectively, the amplitude of TM and TE modes of arm 1 of the Mach-Zehnder modulator can be directly deduced from Eqs. (4.7),

$$A_1'(z) = \frac{1}{\sqrt{2}}(A_0 \cos \kappa z - iB_0 \sin \kappa z), \tag{4.8a}$$

$$B_1'(z) = \frac{1}{\sqrt{2}}(-iA_0 \sin \kappa z + B_0 \cos \kappa z), \tag{4.8b}$$

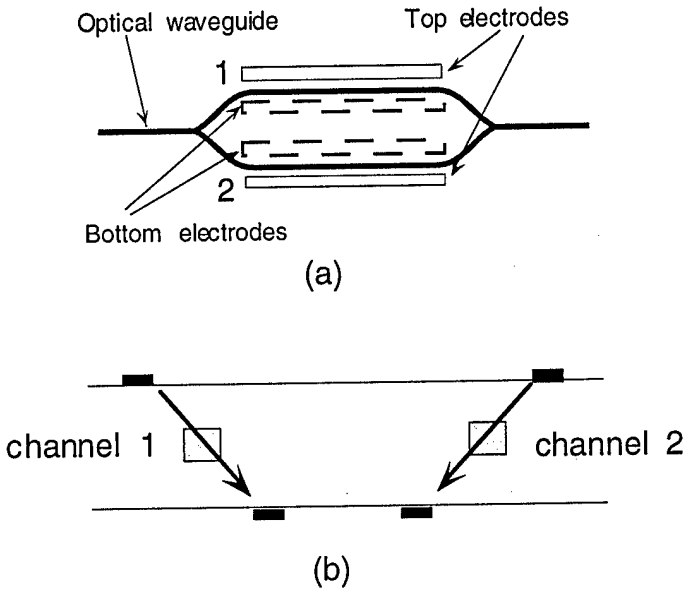

FIGURE 4.2. Polarization-independent Mach-Zehnder modulator. (a) over view, (b) cross-sectional view

For arm 2, due to the change of sign of κ, we have

$$A_2'(z) = \frac{1}{\sqrt{2}}(A_0 \cos \kappa z + iB_0 \sin \kappa z), \tag{4.9a}$$

$$B_2'(z) = \frac{1}{\sqrt{2}}(A_0 i \sin \kappa z + B_0 \cos \kappa z). \tag{4.9b}$$

There are two ways to operate this device. One is common-mode operation, the other is diferential-mode operation. The characteristics of these two modes of operation is discussed below.

4.3.2 Common-mode operation

If the polarity of the modulation electric field is the same with respective to the poling field in the two channels, then the phase factors in Eqs. (4.5) are the same for both of the arms. The complex amplitudes of the TE and TM modes at the output are

$$A_{TE} = \frac{1}{\sqrt{2}}(B_1'(L) + B_2'(L))e^{-i\bar{\beta}L} = B_0 \cos\kappa L e^{-i\bar{\beta}L},$$
$$A_{TM} = \frac{1}{\sqrt{2}}(A_1'(L) + A_2'(L))e^{-i\bar{\beta}L} = A_0 \cos\kappa L e^{-i\bar{\beta}L}.$$

If we denote the input light intensities of TM and TE modes as I_{TM0} and I_{TE0} respectively, the output light intensities for TE and TM mode are

$$I_{TE} = (B_0 \cos\kappa L)^2 = I_{TE0}\cos^2\kappa L, \quad (4.10a)$$
$$I_{TM} = (A_0 \cos\kappa L)^2 = I_{TM0}\cos^2\kappa L. \quad (4.10b)$$

Denote the total input light intensity as $I_0 = I_{TE0} + I_{TM0}$, then the total output intensity is

$$I = I_{TE} + I_{TM} = I_0 \cos^2\kappa L \quad (4.10c)$$

We draw Eqs. (4.10a) and (4.10b) in Fig. 3. One can see that this device is not only polarization indepedent for common-mode operation (Eq. (4.10c)), but also polarization preserving.

The efficiency of modulation is obtained by comparing the driving voltage for this device with that of a conventional push-pull Mach-Zehnder modulator that uses only the maximum component of electro-optic coefficients r_{33}. We define

$$V_\pi = \frac{2\lambda d}{n^3 r_{33} L} \quad (4.11)$$

as the voltage required to generate π phase difference between the two arms in a conventional Mach-Zehder modulator, where d is the distance between the electrodes. The on-off switching voltage for the common-mode operation of our device is found to be

$$V_s = 3V_\pi \quad (4.12)$$

by using Eq. (B1) and assuming $r_{33}=3r_{13}$.

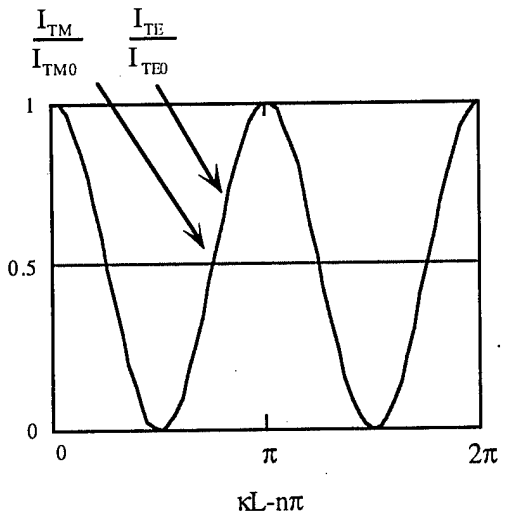

FIGURE 4.3. The transfer curves of TE and TM modes totally overlap with each other for common-mode operation

4.3.3 Differential-mode operation

For differential-mode operation, a bias voltage needs to be applied in order to make $\sin\kappa L=0$, which requires $\kappa L=m\pi$ (m is an integer). If the polarity of the modulation electric field is opposite in sign with respective to the poling field in the two channels, then

$$A_{TM} = \frac{1}{\sqrt{2}}(A_1'(L)e^{-i(\bar{\beta}_0+\Delta\bar{\beta})L} + A_2'(L)e^{-i(\bar{\beta}_0-\Delta\bar{\beta})L})$$
$$= ((-1)^m A_0\cos\Delta\kappa L - iB_0\sin\Delta\kappa L)e^{-i\bar{\beta}_0 L}\cos\Delta\bar{\beta}L$$

$$A_{TE} = \frac{1}{\sqrt{2}}(B_1'(L)e^{-i(\bar{\beta}_0+\Delta\bar{\beta})L} + B_2'(L)e^{-i(\bar{\beta}_0-\Delta\bar{\beta})L})$$
$$= (-iA_0\sin\Delta\kappa L + (-1)^m B_0\cos\Delta\kappa L)e^{-i\bar{\beta}_0 L}\cos\Delta\bar{\beta}L$$

where $\Delta\kappa$ and $\Delta\bar{\beta}$ are modulation electric field induced coupling coefficient and average propagation constant change respectively.

$$I_{TE} = [(A_0\sin\Delta\kappa L)^2 + (B_0\cos\Delta\kappa L)^2]\cos^2\Delta\bar{\beta}L \qquad (4.13a)$$
$$= (I_{TM0}\sin^2\Delta\kappa L + I_{TE0}\cos^2\Delta\kappa L)\cos^2\Delta\bar{\beta}L$$

$$I_{TM} = [(A_0 \cos \Delta\kappa L)^2 + (B_0 \sin \Delta\kappa L)^2] \cos^2 \Delta\bar{\beta} L$$
$$= (I_{TM0} \cos^2 \Delta\kappa L + I_{TE0} \sin^2 \Delta\kappa L) \cos^2 \Delta\bar{\beta} L \qquad (4.13b)$$

Then the total output intensity is

$$I = I_{TE} + I_{TM} = I_0 \cos^2 \Delta\bar{\beta} L. \qquad (4.13c)$$

One can see from Eqs. (4.13c) that the total output intensity is independent of the input polarization state although the output of each polarization is dependent on (see Eqs.(4.13a),(4.13b)). The normalized output light intensities of TE and TM modes and the their sum are shown in Fig. 4 with A_0=0.6 and B_0=0.8.

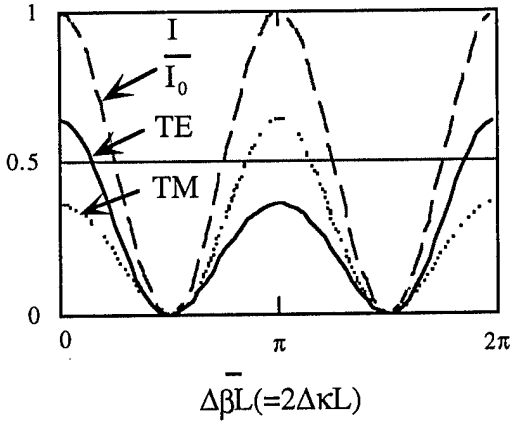

FIGURE 4.4. The curves of I_{TE}/I_o and I_{TE}/I_o are dependent on the polarization of the input, but I/I_0 is not (A_{TEo} =0.6, B_{TEo}=0.8)

The switching voltage can be estimated from Eq. (B2) to be

$$V_s = \tfrac{3}{2} V_\pi.$$

with r_{33}=3r_{13} assumed. This switching voltage is the lowest possible for polarization-insensitive devices, since it is just the average of the switching voltages for separately driving TE and TM modes.

4.3.4 Fabrication-tolerance analysis

A useful device design has to have a fabrication tolerance within the limit of present technology. This design uses a Mach-Zehnder device structure that has much better fabrication tolerance than

directional couplers. The requirement that $\delta=0$ certainly puts new restrictions on the fabrication. For $\delta \neq 0$, Eqs. (4.6) should be used instead of Eqs. (4.7) in the analysis. There will be some additional terms in Eqs. (4.10). These terms cause the output not to be zero when it should be according to Eqs. (4.10) as $\kappa L=(m+1/2)\pi$. We can prove that the ratio of the output light intensity I to the input light intensity I_0 is

$$\frac{I}{I_0}=\frac{\delta^2}{\kappa^2+\delta^2}\approx\frac{\delta^2}{\kappa^2}. \tag{4.15}$$

for common-mode operation, and

$$\frac{I}{I_0}=\frac{\delta^2}{2(\kappa^2+\delta^2)}\approx\frac{\delta^2}{2\kappa^2}. \tag{4.16}$$

for differential-mode operation.

A complete analysis of the effects of the misalignment of the electrodes on the performance of the device is tedious and also requires numerical simulation. But we can get some idea about how the fabrication errors affect δ and hence the device performance by investigating an simplified case as shown in Fig. 3. In this case, we assume a nearly uniform poling electric-field distribution in the waveguide region with an average tilt angle of 45°. We further assume that the waveguide has a square cross-section and that the NLO polymer is isotropic before poling, so we have $\beta_a=\beta_a$ and $\kappa_{aa}=\kappa_{ab}$ because of symmetry. Then Eq. (A16) gives $\delta=0$. However, if there is a horizontal misalignment Δ in the relative position of the poling electrodes, Eq. (A16) leads to

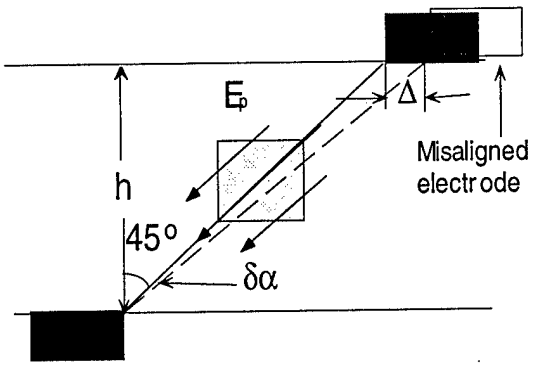

FIGURE 4.5 The effect of misaligned electrode on the tiltness of poling field

$$\delta = \frac{(\beta_a + \kappa_{aa}) - (\beta_b + \kappa_{bb})}{2} = \frac{\kappa_{aa} - \kappa_{bb}}{2}.$$

Adopting uniformity assumption of the poling-electric field and using Eqs. (A9), we get approximately

$$\delta \approx \frac{\pi}{\lambda}(n_1^2 - n_2^2)\cos 2\alpha, \tag{4.17}$$

$$\kappa \approx \frac{\pi}{2\lambda}(n_1^2 - n_2^2). \tag{4.18}$$

So $$\frac{\delta}{\kappa} = 2\cos 2\alpha \approx 4(\delta\alpha), \tag{4.19}$$

which are independent of the magnitude of the birefringence and are dependent only on the deviation of the tilting angle from the 45° line. Trigonometric analysis shows

$$\delta\alpha \approx \frac{\Delta}{2h}, \tag{4.20}$$

where h is the vertical separation of the poling electrodes as shown in Fig. 5. We then get

$$\frac{I}{I_0} \approx 4(\frac{\Delta}{h})^2 \tag{4.21}$$

for common-mode operation, and

$$\frac{I}{I_0} \approx 2(\frac{\Delta}{h})^2 \tag{4.22}$$

for differential-mode operation. These equations show that this design has good fabrication tolerance. In most practical devices, h is no less than 10 μm, so even with 0.5 μm fabrication error a 20 dB extinction ratio can be achieved.

4.4. CONCLUSION

We have analyzed the effect of tilted-poling-induced birefringence on the polarization conversion in single TE and TM mode waveguides by coupled-mode theory. A polarization-independent electro-optic

modulator with continuous electrodes is designed by using the deduced formulae. This device uses a Mach-Zehnder structure with two arms poled in a tilted fashion. It can be operated in common mode or differential mode. The output under common-mode operation has the attribute of being polarization preserving, although propagation through each arm of the modulator is not polarization preserving. The output under differential-mode operation has the attribute over the other mode of operation of requiring only half the driving voltage, however it is not polarization preserving. For both modes of operation, 100% switching contrast is achievable under idealized fabrication conditions. The sensitivity to fabrication error is proven to be small, and anticipated not to be a problem with present micro-fabrication technonlogy.

4.5. APPENDICES

4.5.1 Appendix A

Using the identity

$$\nabla \times \nabla \times \mathbf{E} = \nabla(\nabla \cdot \mathbf{E}) - \nabla^2 \mathbf{E},$$

we can rewrite Eq. (3) as

$$\nabla^2 \mathbf{E} + \frac{\omega^2}{c^2} \varepsilon_{\mathbf{r}} \cdot \mathbf{E} = \nabla(\nabla \cdot \mathbf{E}). \tag{A1}$$

Since $\nabla \cdot \mathbf{E}_x(x,y,z) = 0$ and $\nabla \cdot \mathbf{E}_y(x,y,z) = 0$, we have

$$\nabla(\nabla \cdot \mathbf{E}) = \nabla(\nabla A(z) \cdot \mathbf{E}_x(x,y,z) + \nabla B(z) \cdot \mathbf{E}_y(x,y,z)) \text{ and} \tag{A2}$$

$$\nabla^2 \mathbf{E}_x(x,y,z) + \frac{\omega^2}{c^2} \varepsilon_{xx} \mathbf{E}_x(x,y,z) = 0 \tag{A3a}$$

$$\nabla^2 \mathbf{E}_y(x,y,z) + \frac{\omega^2}{c^2} \varepsilon_{yy} \mathbf{E}_y(x,y,z) = 0, \tag{A3b}$$

where ε_{xx} and ε_{yy} are the components of dielectric-contant matrix of the waveguide before poling. Ignoring the z component of $\mathbf{E}_x(x,y,z)$ and $\mathbf{E}_y(x,y,z)$, we write

$$\mathbf{E}_x(x,y,z) = E_x(x,y) e^{i(\omega t - \beta_a z)} \hat{\mathbf{x}}, \tag{A4a}$$

$$\mathbf{E}_y(x,y,z) = E_y(x,y) e^{i(\omega t - \beta_b z)} \hat{\mathbf{y}}. \tag{A4b}$$

Using Eqs. (1)-(3), Eqs. (A1)-(A4), and the assumption

$$\frac{\partial^2 A(z)}{\partial z^2} << k\frac{\partial A(z)}{\partial z}, \tag{A5a}$$

$$\frac{\partial^2 B(z)}{\partial z^2} << k\frac{\partial B(z)}{\partial z} \tag{A5b}$$

of slow variation of mode amplitudes over z, we obtain the following equations by neglecting the second-derivatives of $A(z)$ and $B(z)$,

$$-2i\beta_a \frac{dA}{dz}E_x e^{i(\omega t-\beta_a z)} + \frac{\omega^2}{c^2}(\varepsilon_{11}-\varepsilon_{xx})AE_x e^{i(\omega t-\beta_a z)} + \frac{\omega^2}{c^2}\varepsilon_{12}BE_y e^{i(\omega t-\beta_b z)} = \frac{dA}{dz}\frac{\partial E_x}{\partial x}e^{i(\omega t-\beta_a z)} + \frac{dB}{dz}\frac{\partial E_y}{\partial x}e^{i(\omega t-\beta_b z)}, \tag{A6a}$$

$$-2i\beta_b \frac{dB}{dz}E_y e^{i(\omega t-\beta_b z)} + \frac{\omega^2}{c^2}\varepsilon_{21}AE_x e^{i(\omega t-\beta_a z)} + \frac{\omega^2}{c^2}(\varepsilon_{22}-\varepsilon_{yy})BE_y e^{i(\omega t-\beta_b z)} = \frac{dA}{dz}\frac{\partial E_x}{\partial y}e^{i(\omega t-\beta_a z)} + \frac{dB}{dz}\frac{\partial E_y}{\partial y}e^{i(\omega t-\beta_b z)}. \tag{A6b}$$

Using the normalization

$$\int E_i^* E_i dxdy = \frac{2\omega\mu}{|\beta_i|},\ i=x,y, \tag{A7}$$

we deduce from Eqs. (6) that

$$(1+i\kappa_{aa'})\frac{dA}{dz} + i\kappa_{ab'}\frac{dB}{dz}e^{i(\beta_a-\beta_b)z} = -i\kappa_{aa}A - i\kappa_{ab}Be^{i(\beta_a-\beta_b)z}, \tag{A8a}$$

$$i\kappa_{ba'}\frac{dA}{dz}e^{-i(\beta_a-\beta_b)z} + (1+i\kappa_{bb'})\frac{dB}{dz} = -i\kappa_{ba}Ae^{-i(\beta_a-\beta_b)z} - i\kappa_{bb}B, \tag{A8b}$$

where

$$\begin{aligned}
\kappa_{ab} &= \kappa_{ba}^* = \frac{\omega\varepsilon_0}{4}\int E_x^*\varepsilon_{12}E_y dxdy,\\
\kappa_{aa} &= \frac{\omega\varepsilon_0}{4}\int E_x^*(\varepsilon_{11}-n_x{}^2)E_x dxdy,\\
\kappa_{bb} &= \frac{\omega\varepsilon_0}{4}\int E_y^*(\varepsilon_{22}-n_y{}^2)E_y dxdy,\\
\kappa_{ab'} &= \frac{\omega\varepsilon_0}{4}\int E_x^*\frac{\partial E_y}{\partial x}dxdy,\\
\kappa_{ba'} &= \frac{\omega\varepsilon_0}{4}\int E_y^*\frac{\partial E_x}{\partial y}dxdy,\\
\kappa_{aa'} &= \frac{\omega\varepsilon_0}{4}\int E_x^*\frac{\partial E_x}{\partial x}dxdy,\\
\kappa_{bb'} &= \frac{\omega\varepsilon_0}{4}\int E_y^*\frac{\partial E_y}{\partial y}dxdy.
\end{aligned} \tag{A9}$$

Simple integration shows that $\kappa_{aa'} = \kappa_{bb'} = 0$. The coefficients $\kappa_{ab'}$ and $\kappa_{ba'}$ are much smaller than unity and vanish when the unpoled waveguides are symmetric in both x and y directions. For simplicity, we restrict our discussion to this symmetric case. Then Eqs. (A8) reduce to

$$\frac{dA}{dz} = -i\kappa_{aa}A - i\kappa_{ab}Be^{i(\beta_a-\beta_b)z}, \tag{A10a}$$

$$\frac{dB}{dz} = -i\kappa_{ba}Ae^{-i(\beta_a-\beta_b)z} - i\kappa_{bb}B. \tag{A10b}$$

Equations. (A10) are the standard coupled-mode equations. By the following substitution

$$A(z) = e^{-i\kappa_{aa}z+i\delta z}A'(z), \tag{A11a}$$

$$B(z) = e^{-i\kappa_{bb}z-i\delta z}B'(z), \tag{A11b}$$

we have

$$\mathbf{E} = [A'(z)E_x(x,y)\hat{\mathbf{x}} + B'(z)E_y(x,y)\hat{\mathbf{y}}]e^{i(\omega t-\bar{\beta}z)}, \tag{A12}$$

$$\begin{pmatrix} A'(z) \\ B'(z) \end{pmatrix} = \begin{bmatrix} S & -iX \\ -iX^* & S^* \end{bmatrix} \begin{pmatrix} A(0) \\ B(0) \end{pmatrix}, \tag{A13}$$

where

$$S = \cos(z\sqrt{\kappa^2+\delta^2}) - \frac{i\delta}{\sqrt{\kappa^2+\delta^2}}\sin(z\sqrt{\kappa^2+\delta^2}) \tag{A14a}$$

$$X = \frac{\kappa}{\sqrt{\kappa^2+\delta^2}}\sin(z\sqrt{\kappa^2+\delta^2}) \tag{A14b}$$

$$\kappa = \kappa_{ab} = \kappa_{ba}^* \tag{A15}$$

$$\delta = \frac{(\beta_a+\kappa_{aa})-(\beta_b+\kappa_{bb})}{2} \tag{A16}$$

$$\bar{\beta} = \frac{(\beta_a+\kappa_{aa})+(\beta_b+\kappa_{bb})}{2}. \tag{A17}$$

4.5.2 Appendix B

Assuming a square cross-section of the waveguide and a uniform poling electric field with 45° tilting , we have

$$\kappa = \frac{\omega\varepsilon_0}{4}\int E_x^*(n_1^2-n_2^2)\sin\alpha\cos\alpha E_y dxdy$$

$$\approx \frac{\omega\varepsilon_0}{4}\int E_x^* E_y dxdy \cdot \frac{1}{2}(n_1^2-n_2^2)$$

Considering that E_x and E_y should have quite similar distributions because of the symmetry, and using the normalization equation (A7) and $\beta \approx nk = \frac{2\pi}{\lambda}n$, we then have

$$\kappa \approx \frac{k}{4n}(n_1^2 - n_2^2) = \frac{\pi}{2\lambda n}(n_1^2 - n_2^2).$$

The modulation electric field E induced change in κ is

$$\Delta\kappa = \frac{\pi}{\lambda}(\Delta n_1 - \Delta n_2) = -\frac{\pi}{3\lambda} n^3 r_{33} E, \qquad \text{(B1)}$$

where we have used the assumption $r_{33} = 3r_{13}$ and $\Delta n_1 = -\frac{1}{2} n^3 r_{33} E$ and $\Delta n_2 = -\frac{1}{2} n^3 r_{13} E$. Similarly we can deduce the induced change in $\bar{\beta}$ by modulation electric field E

$$\Delta\bar{\beta} \approx \frac{\pi}{\lambda}(\Delta n_1 + \Delta n_2) = -\frac{2\pi}{3\lambda} n^3 r_{33} E. \qquad \text{(B2)}$$

5. Device Fabrication

5.1 FABRICATION OF DIRECTIONAL COUPLERS

The following steps are taken in the fabrication of a directional coupler. First, a bottom cladding layer of NOA-61 is spun onto a silicon wafer to form a 3-μm layer. The NOA-61 layer is then cured with UV light. Next, LD-3 is spin coated onto the NOA-61 layer. This results in an LD-3 layer with a thickness of 1.2 μm. The LD-3 layer is poled and cured. AZ5209 photoresist is then spun onto the LD-3 layer and patterned using the mask for the directional coupler. The sample is then developed with AZ425 developer and reactive ion etched to define the channel waveguide regions. A top NOA-61 cladding is then applied to the sample and cured. The silicon wafer is then scribed and cut, so that the ends of the device are at the edges of the wafer. The input and output ends are then polished using a Beuhler polisher with diamond abrasive films of various grits. First, a 9 μm diamond abrasive film is used for ten minutes at 90 revolutions per minute. Then an abrasive film of 6 μm grit is used for seven minutes at 70 RPM. Next, a film of 3 μm grit is used for three minutes at 40 RPM. Finally, a 1 μm grit film is used for one minute at 30 RPM. For all the films, a Kimwipe® is used to clean the abrasive film of the residue being removed from the sample. The polishing resulted in a smooth interface for coupling. A schematic of the cross section of the input to the directional coupler is shown in Fig. 5.1.

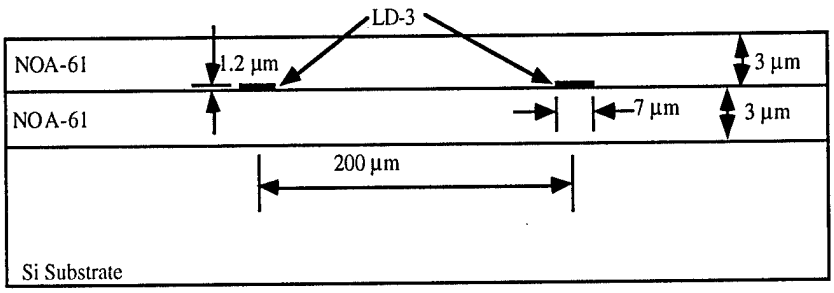

FIGURE. 5.1. Schematic of cross section of the input.

A photograph of the output end of a directional coupler device was taken using a digital SPOT® camera. The channels have a center-to-center separation of 18 μm and are the dark colored trapezoids in the picture. The right channel is outlined with a white trapezoid to assist in identifying the LD-3 channel waveguides. The photograph is shown in Fig. 5.2.

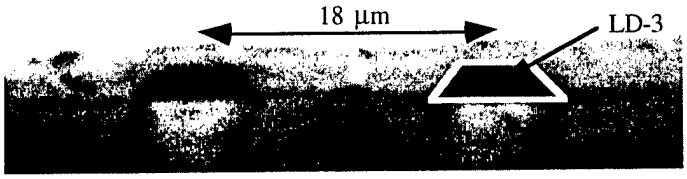

Fig. 5.2. Photograph of output cross section

For the fabrication of an active device, electrodes need to be patterned above and below the channel waveguide regions. This is accomplished by first evaporating a metal such as gold or aluminum onto the silicon substrate. The electrode region is then patterned and defined using another mask made specifically for the electrode structure. The spin coating of the bottom NOA-61 layer, LD-3 layer, and top NOA-61 layer are all done as previously described. Finally, a top metal layer of gold or aluminum is evaporated and patterned onto the top NOA-61 layer. For an active device, the cladding regions should be as thin as possible, so that lower modulation voltages can be used. A schematic of an active device is shown in Fig. 5.3.

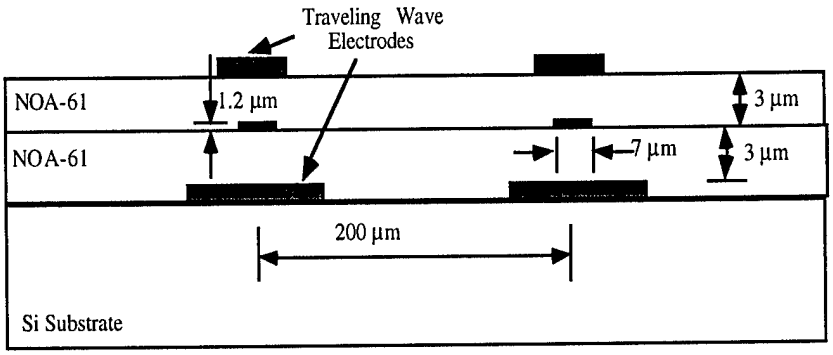

FIGURE 5.3. Schematic of cross section of an active device.

5.2 FABRICATION OF POLARIZATION-INSENSITIVE MACH-ZEHNDER MADULATORS

A direct thought to fabricate polarization-insinsitive polymer modulators is to use a combination of in-plane poling and vertical poling. The ratio of induced phase change of TE mode to TM mode is 3:1 in the in-plane poled region, while in the vertical poled region is 1:3. When light passes through the two regions, the phase modulation to TE mode and TM mode though is not the same in each region, but the average effect of these two region can be the same. The fabrication process is as follow: Bottom electrodes are deposited on quartz substrates and patterned by photolithography, then NOA61 cladding, LD-3 polymer and NOA61 cladding layers are sequentially deposited by spincoating. In-plane poling and vertical poling are performed simultaneously by applying the poling voltage across the electrodes. The same electrodes are used for the electro-optic modulation. Figure 5.4 (a) and (b) show how to achieve in-plane poling and vertical poling on the same substrate. Fig. 5.4 (c) shows how these two regions are connected. Fig. (d) shows the Y-branch region of the waveguide. The design idea of this device is simple. However, it does have limitations at very high speed operation. As mentioned in section 4.1, the non-continuous electrodes are very difficult to be used in traveling-wave modulation, hence the device speed will be limited by the RC constant of the modulation electric circuit. A new design and fabrication process is under way using the result of chapter 4 of this report.

6. Conclusion

We invented a new poling method--high temperature liquid contact poling (HTLCP)–which is an important contribution to the development of nonlinear optical polymers. We have solved the crosslinker crystallization problem which has botherd other researchers for several years. A new method of electro-optic measurenment is invented which has

the advantageof being able to measure r_{33} and r_{13} separately with relative high accuracy. A theory of TE–TM mode conversion in tilted-poled NLO waveguides is developed. A new polarization-independent Mach–Zehnder modulator is designed by using this theory. This device uses continuous modulation electrodes, thereby allowing to use traveling-wave modulation to achieve extremely high speed. Primary polarization-independent devices and directional-coupler devices have been fabricated. Design and fabrication of new high performance electro-optic devices are under way.

7. PUBLICATIONS

1. Huajun Tang, Guohua Cao, John M. Taboada, Ray T. Chen, "Improved optical quality of crosslinkable nonlinear polymer waveguides by anchoring the diffusive small molecules", Journal of Polymer Science, B Polymer Physics (In press)

2. Huajun Tang, Guohua Cao, John M. Taboada, Ray T.Chen, "Inverse poling techniques for polymer electrooptic switches" *Optoelectronic Integrated Circuits,* Yoon-Soo Park and Ramu V. Ramaswamy, Ed., SPIE Proceeding 3006-51, February 1997

3. Huajun Tang, Guohua Cao, John M. Taboada, Ray T.Chen, "Fabrication of high quality optical polymer multilayer films on silicon substrates," *Silicon-based Monolithic and Hybrid Optoelectronic Devices*, Derek C. Houghton and Bahram Jalali, Ed., SPIE Proceeding 3007-19, February, 1997

4. Huajun Tang, Jeffery J. Maki, and Ray T. Chen, "Analysis Of Poling Induced Birefringence On The Design Of Polarization-Independent Nonlinear Optical Polymeric Devices", *Polarization,;measurement, analysis, and remote sensing*, Dennis H. Goldstein and Russell A. Chipman, Ed., SPIE Proceeding 3121-33, August, 1997

5. Huajun Tang, Jeffery J. Maki, John M. Taboada, Guohua Cao, Degui Sun, and Ray T. Chen, "Novel Poling and Electro-Optic Measurement Methods of Cladded Nonlinear-Optical Polymer Films", *Nonlinear optical properties of organic materials*, Mark G. Kuzyk, Ed., SPIE Proceeding 3147-20, August, 1997

6. John M. Taboada, Huajun Tang, Guohua Cao, Zhuzhou Yue, Ray T.Chen, "Fabrication of reversed Δß polymer electrooptic switches", *Physics and Simulation of Optoelectronic Devices,* Marek Osinski and Weng W. Chow, Ed., SPIE proceeding 2994-39, February, 1997.

7. Huajun Tang, Guohua Cao, John M. Taboada, Jeffery M. Maki, Ray T.Chen, "Polymer Mach-Zehnder modulators for optical interconnects", PhotonicsWest'98, San Jose, February, 1998 (to be published)

8. REFERENCES

CHAPTER 2

2.1 R.A. Norwood, T.Findakly, H. A. Golberg, G. Khanarian, J. B. Stamatoff, and H.N.Yoon, *Polymers for lightwave and integrated optics*, L.A. Hornak, Ed., Marcel Dekker, Inc., New York, 1992, part II

2.2 T.C. Kowalczyk, T.Z.Kosc, K.D.Singer.A.J.Beuhler D.A.wargoski, P.A.Cahill, C.H.Seager,and M.B. Meihardt, J.Appl.Phys. **78**, 5876 (1995)

2.3 E.M.Cross, K.M.white, R.S.Moshrefzadeh, C.V. Francis, Macromolecules, **28**, 2526 (1995)

2.4 C.Xu, B. Wu, O. Todorava and L.Dalton and Y. Shi, P. M. Ranon and W.H. Steier, Macromolecules **26**, 5303 (1993)

2.5 R. Levenson, J.Liang, C. Rossier, R. Hierle, E. Taussaere, N. Bouadma and J. Zyss, *Polymer for second-order nonlinear optics,* G.A. Lindsay AND K.D.Singer, American Chemical society, Washington, DC, 1995), p436

2.6 G.F. Lipscomb, R. S. Lytel, A.J. Tickmnor, T. E. Van Eck, S.L. Kwinatwowski, and D.G. Girton, *Proc. SPIE* , **1337**, 23 (1990).

2.7 Peter M.Ranon, Ph.D. dissertation, University of Southern California, 1993. (Note: LD-3 is SC-XL12B)

2.8 J.H.Bechtel, Y.Shi,W.Wang, *Proc. SPIE*, **2690**, 202 (1996)

2.9 W.Wang, D.Chen, H.R.Feterman, Y.Shi, W.H.Steier, L.Dalton, R.-M.D.Chow, Appl. Phys. Lett. **67** (13), 1806 (1995). Also see some of the references.

2.10 H. Nishihana, *Optical Integrated Circuits*, McGraw-Hill Book Company, New York, 1987.

CHAPTER 3

3.1. Manfred Eich, Robert Blum, and Martin Sprave, "Electrical conduction processes and high electric field poling nonlinear otical polymers", *Nonlinear optical propeties of organic mtaerials IX*, SPIE **2852**,Gustaaf R. Mohlmann ed. p64, 1996

3.2. T. C. Kowalczyk, T. Z. Kosc, K. D. Singer, A. J. Beuhler, D. A. Wargoski, P. A. Cahill, C. H. Seager and M. B. Meinhardt, "Crosslinked polyimide electro-optic materials," *J. Appl. Phys.* **78**, 5876 (1995).

3.3. J. S. Schildkraut, "Determination of the electrooptic coefficient of a poled polymers," *Appl. Opt.* **29**, 2839 (1990).

3.4. C. C. Teng and H. T. Man, "Simple reflection technique for measuring the electro-optic coefficient of poled polymers," *Appl. Phys. Lett.* **56**, 1734 (1990).

3.5. H.R.Cho, M.J. Shin, S.H. Han, and J.W. Wu, "Mach-Zehnder interferometer measurement of Pockels effect in a poled polymer film with a coplanar electrode structure", Appl. Phys. Lett. **69**(25), p.3788, 1996

3.6. P.M.Lunquist, M.Jurich, J.-F. Wang, H . Zhou T.J. Marks and G.K. Wong, "Electro-optical characterization of poled-polymer films in transmission, Appl. Phys. Lett. **67**(7), 901 (1996)

3.7. Yongqian Shi, David J. Olson, and J. H. Bechtel, "Wavelength dependent photoinduced depoling in poled nonlinear optical polymer thin films", *Nonlinear optical propeties of organic mtaerials VII*, SPIE **2827**,Gustaaf R. Mohlmann, p.200, 1995.

3.8. Mehrdad Ziari, Srinath Kalluri, Sean Garner, William H. Steier, Zhiyong lIang, Larry R. Dalton and Yongqiang Shi, "Novel electro-optic measurement techniqes for coplanar electrode poled polymers, *Nonlinear optical propeties of organic mtaerials VII*, SPIE **2827**,Gustaaf R. Mohlmann, p.218, 1995.

3.9. R. A. Hill, A. Knoesen and M. A. Mortazavi, "Corona poling of nonlinear polymer thin films for electro-optic modulators," *Appl. Phys. Lett.* **65**, 1733 (1994).

3.10. M. A. Mortazavi, A. Knoesen, S. T. Kowel, B. G. Higgins, and A. Dienes, "Second-harmonic generation and absorption studies of polymer-dye films oriented by corona-onset poling at elevated temperatures," *J. Opt. Soc. Am.* B **6**, 733 (1989).

3.11. Huajun Tang, John M. Taboada, Guohua Cao, Liqiang Li, and Ray T. Chen, "Enhanced electro-optic coefficient of nonlinear optical polymer using liquid contact poling", *Appl. Phys. Lett.* **70**(5), 538(1996)

3.12. Huajun Tang, Guohua Cao, John M. Taboada, Ray T. Chen, "Improved Optical Quality of Crosslinkable Nonlinear Polymer Waveguides by Anchoring the Diffusive Small Molecules", accepted by *J. Polymer Science, 1997*

CHAPTER 4

4.1. Min-cheol Oh and Sang-Yung Shin, "Ploymeric polerization-independent modulator incorporating twisted optic-axis waveguide polarization convertors", *IEEE Photon.Technol. Lett.*, **8**(11), 1483 (1996)

4.2. T. Gase, Abrauer, W. Karthe, "Polarization insinsitive phase modulator based on polymers for hybrid integration", ECI)'95 Proceedins, *7th European Conference on Integrated Optics with Technique Exibition*, p85, 1995.

4.3. William R. Holland, "Fabrication and characterization of polymeric lightwave devices", in *Polymers for lightwave and integrated optics,* L.A. Hornak, Ed., Marcel Dekker, Inc., New York, 1992, p410

4.4. Wol-Yon Hwang, Jang-Joo Kin, Taehyoung, MinCheol Oh, and Sang-Yung Shin, "TE-TM mode convertor in a poled polymer waveguide", J.Quantum Electron. 32(6), 1054(1996).

4.5. Min-Cheol, Sang-Shin Lee, and Sang-Yung Shin, "Simulation of polarization converter formed by poling-induced polymer waveguides", IEEE J. Quant.Electron. 31(9), p1698-1704, 1995 `

4.6. Amnon Yariv and Pochi Yeh, *Optical Waves in Crystals*, John Wiley & Sons, New York, p 459, 1984.